Solar-Terrestrial Physics. 2024. Vol. 10. Iss. 2. P. 26–33. DOI: 10.12737/stp-102202403. © 2024
I.I. Kovalev, M.V. Kravtsova, S.V. Olemskoy, V.E. Sdobnov, S.A. Starodubtsev. Published by INFRA-M Academic Publishing House

UDC 524.1-550.3
DOI: 10.12737/stp-102202403

Received January 09, 2024
Accepted March 26, 2024

MONITORING OF NEAR-EARTH SPACE, EARTH'S MAGNETOSPHERE AND ATMOSPHERE DURING FORBUSH DECREASES IN AUGUST 2005

I.I. Kovalev
Institute of Solar-Terrestrial Physics SB RAS, Irkutsk, Russia, ivankov@iszf.irk.ru

M.V. Kravtsova
Institute of Solar-Terrestrial Physics SB RAS, Irkutsk, Russia, rina@iszf.irk.ru

S.V. Olemskoy
Institute of Solar-Terrestrial Physics SB RAS, Irkutsk, Russia, osv@iszf.irk.ru

V.E. Sdobnov
Institute of Solar-Terrestrial Physics SB RAS, Irkutsk, Russia, sdobnov@iszf.irk.ru

S.A. Starodubtsev
Yu.G. Shafer Institute of Cosmophysical Research and Aeronomy SB RAS, Yakutsk, Russia, starodub@ikfia.sbras.ru

Abstract. We present the results of near-Earth interplanetary space, magnetosphere, and atmosphere monitoring during large-scale solar wind disturbances at the end of August 2005. The monitoring was carried out using ground-level cosmic ray (CR) observations made at the worldwide network of neutron monitors as well as muon telescopes in Yakutsk and Novosibirsk. As a result of the analysis performed by different methods, we have obtained variation properties of CRs of different rigidities in Earth's orbit, their pitch angle anisotropy, orientation and configuration of the interplanetary magnetic field, changes in the planetary system of geomagnetic cutoff rigidities during geomagnetic disturbances, as well as mass average air temperature over CR stations equipped with muon telescopes. For the periods of geomagnetic disturbances, we have determined parameters of magnetospheric ring current and magnetopause currents.

Keywords: cosmic rays, Forbush effect, magnetosphere, atmosphere.

INTRODUCTION

An actual direction of recent research into variations in the intensity of galactic cosmic rays (GCRs) is the study of conditions of the heliosphere, magnetosphere, and atmosphere from ground-based measurements of CR fluxes. The observed CR variations are an integral result of CR flux modulation due to various physical phenomena on the Sun, in the heliosphere, Earth's magnetosphere and atmosphere. The CR intensity measured on the Earth surface depends on meteorological parameters (such as temperature and air pressure), geomagnetic field conditions, as well as on the so-called space weather — physical conditions on the Sun and in the heliosphere. Accordingly, CR variations can be divided into three classes: I — of meteorological origin, II — driven by geomagnetic field variations, and III — caused by changes in space weather that is governed by solar activity. The last class of CR variations includes sporadic ground level enhancements of the solar CR (SCR) flux and decreases in the GCR intensity, known as Forbush effects (FE) [Forbush, 1937; Belov et al., 2001], which are often accompanied by geomagnetic disturbances.

When using ground-based observations of CRs to solve problems related to monitoring phenomena in the interplanetary medium, Earth's magnetosphere and atmosphere, there is a need for continuous recording of the intensity of different CR components and special data processing techniques, which allow us to utilize the entire worldwide network of stations as a single multichannel and multi-directional device.

In this work, using observations of the CR intensity from the worldwide network of neutron monitors (NM), as well as measurements with muon telescopes (MT) at the stations Yakutsk and Novosibirsk, we examine variations in the rigidity spectrum, GCR anisotropy, changes in the planetary system of geomagnetic cutoff rigidity, as well as temperature characteristics of the atmosphere in Yakutsk and Novosibirsk in late August 2005.
The time period in question is characterized by significant energy release in active region (AR) 10798, which appeared in the center of a small coronal hole (CH). Features of the evolution of AR 10798 have been detailed in [Asai et al., 2009]. This AR gave rise to three Class M flares. Two flares occurred on August 22, 2005: the first (S11W54) was X-ray class M2.6; the second (S13W65), M5.6. The third flare (S14W90) of the M2.7 class occurred on August 23, 2005. Each flare generated a halo-type coronal mass ejection (CME) [https://cdaw.gsfc.nasa.gov/CME_list/UNIVERSAL_ver1/2005_08/univ2005_08.html]. All the CMEs (let us call them CME-1, CME-2, and CME-3) had high speeds: ~1200, 2400, and 1900 km/s respectively. CME-1 came into the field of view of the LASCO/SOHO coronagraph on August 22, 2005 at 01:31 UT; CME-2, on August 22, 2005 at 17:30 UT; and CME-3, on August 23, 2005 at 14:54 UT. Each of them was associated with a type II radio burst [https://cdaw.gsfc.nasa.gov/CME_list/radio/waves_type2.html]. A radio burst of this type can be considered as an indicator for a propagating shock wave capable of

accelerating particles. CME-2 was especially fast. It was observed approximately 16 hrs after CME-1. When moving toward Earth, CME-2 caught up with slower CME-1 and joined it; then CME-3 occurred. The series of successive high-speed CMEs generated an interplanetary disturbance, in which against the background of a high-speed solar wind (SW) stream (velocity over 700 km/s) (Figure 1, *b*) there was a sharp increase in the interplanetary magnetic field (IMF) modulus to ~55 nT (Figure 1, *a*) and the IMF southward B_z component to –30 nT [https://omniweb.gsfc.nasa.gov]. A quasi-perpendicular interplanetary shock wave (ISW) associated with the CME passage was recorded by the ACE spacecraft, located at the libration point L1, on August 24, 2005 at 05:37 UT and featured a mean angle between the direction of the IMF vector and the normal to the IMF front Θ_{Bn}=64.6° [https://lweb.cfa.harvard.edu/shocks]. It was also detected by the WIND spacecraft, located near the L1 point (Θ_{Bn}=66.8°). On August 24, 2005, a geomagnetic storm began with a minimum *Dst* index of –216 nT (Figure 1, *h*). Simultaneously with the geomagnetic storm, an FE (hereinafter referred to as FE-1) was recoded on Earth with significant amplitudes –6÷–8 % at polar and mid-latitude CR stations.

During the GCR intensity recovery phase on August 30, 2005, a second FE (FE-2) occurred with an amplitude of a CR intensity decrease more than 2 % at high-latitude CR stations, which was also accompanied by a geomagnetic storm with a decrease in the *Dst* index to –131 nT (Figure 1, *h*). According to the WIND data [https://cdaw.gsfc.nasa.gov/CME_list/radio/waves_type2.html], these geoeffective events were related to a post-limb flare, which generated halo-type CME on August 29 at 10:24 UT. Its speed was 1600 km/s. Yet, ACE and WIND did not detect ISW at that time [https://lweb.cfa.harvard.edu/shocks /]. From 11:10 UT, a type II burst was observed in VHF [https://cdaw.gsfc.nasa.gov/CME_list/radio/waves_type2.html]. The interplanetary disturbance manifested itself in an increase in the SW velocity to 460 km/s and the IMF modulus to >17 nT (Figure 1, *a*, *b*) [https://omniweb.gsfc.nasa.gov].

The profiles of FE-1 and FE-2 are different. FE-1 was characterized by a sudden onset and was accompanied by a sharp decrease in the CR intensity, with the IMF B_z component being about –41 nT. FE-2 began gradually and B_z was around –16 nT. Abunin et al. [2012] have demonstrated that sudden-onset FEs are triggered by CMEs, whereas a significant part of gradual-onset events is associated with high-speed plasma flows from CH. In our case, for gradual-onset FE-2 the statement of Abunin et al. [2012] is ambiguous since that time there was a fast halo-type CME in interplanetary space, which might have been related to CH [Verma, 1998; Liu, Hayashi, 2006].

DATA AND METHOD

For the analysis, we have used data averaged over one hour from the worldwide network of NM (44 NM) [https://www.nmdb.eu], corrected for pressure, and MTs at the stations Yakutsk (5 particle arrival directions) [https://ysn.ru/ipm/ykt MT00] and Novosibirsk (22 particle arrival directions) [https://cosmrays.ipgg.sbras.ru]. Modulation amplitudes of the CR intensity were measured from the quiet background level on August 20, 2005.

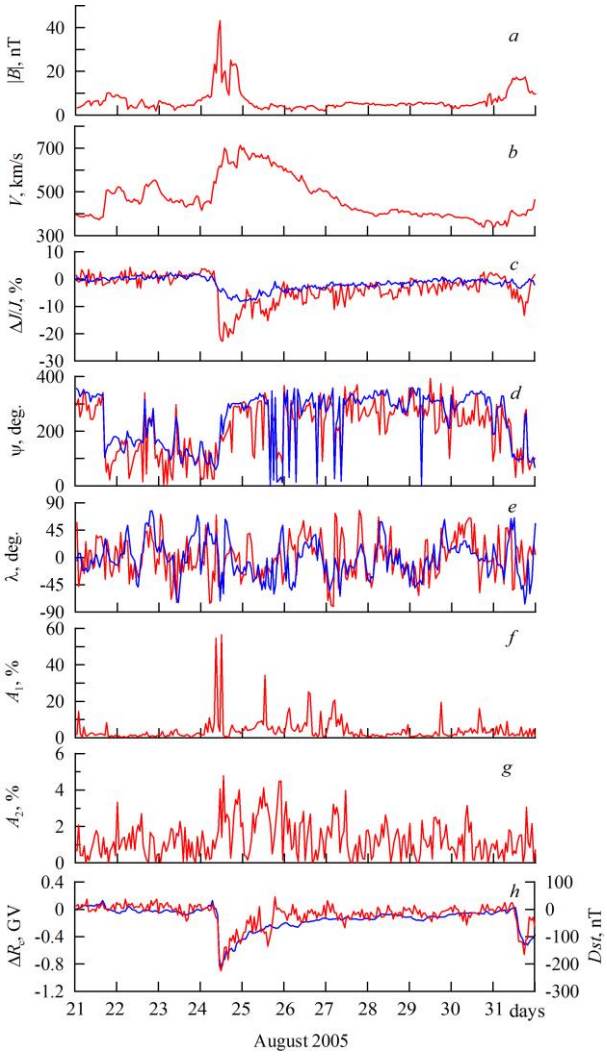

Figure 1. IMF modulus (*a*) and SW velocity (*b*); isotropic component of CR variations (*c*) with 4 GV (red line) and 10 GV (blue line) rigidities; longitude (*d*) and latitude (*e*) IMF orientation angles: the red line indicates calculation by the SGS method; the blue line is experimental data; the first (*f*) and second (*g*) harmonics of pitch-angle anisotropy of CRs with 4 GV rigidity; variations (*h*) of the geomagnetic cutoff rigidity in Irkutsk (red line) and of the *Dst* index (blue line)

To analyze solar activity, IMF, and SW parameters, we have employed the data presented in the catalogs [https://www.solarmonitor.org; https://cdaw.gsfc.nasa.gov; https://lweb.cfa.harvard.edu; https://omniweb.gsfc.nasa.gov].

We analyzed the CR measurements by the spectrographic global survey (SGS) method [Dvornikov, Sdobnov, 1997; Kovalev et al., 2022], which allows us to identify and study variations in the rigidity spectrum and CR anisotropy, changes in the planetary geomagnetic cutoff rigidity system for each measurement hour, as well as to estimate the mass average air temperature at muon observation stations, from ground-based observations. The effectiveness of the SGS method in solving problems of solar-terrestrial physics has been proven in many publications, for example, in [Grigoryev et al.,

2009; Alania et al., 2013; Kichigin et al., 2017; Ptitsyna et al., 2023].

Table 1 lists errors in the values calculated by the SGS method depending on the statistical accuracy of CR intensity observations considered [Kovalev et al., 2022]. Note that these errors are due to the statistical accuracy of the initial data and do not take into account other sources of uncertainty such as model errors and adopted approximations.

The obtained results are interpreted using the model of CR modulation by regular electromagnetic fields of the heliosphere [Dvornikov et al., 2013], developed at the Institute of Solar-Terrestrial Physics SB RAS. Unlike the generally accepted convection-diffusion model [Parker, 1958; Krymsky, 1964] according to which CR modulation is triggered by a change in particle density due to their sweeping out by SW small-scale magnetic inhomogeneities, and the intensity increases during solar flares, by a solar source; CR modulation in our model is induced by a change of particle energy in heliospheric electromagnetic fields of different origin. Our model can explain the high degree of CR anisotropy during SW disturbances and solar proton events (see, e.g., [Dvornikov, Sdobnov, 1997; Richardson et al., 2000]).

To calculate the parameters of magnetospheric current systems — ring current radii in the inner magnetosphere (r_{DR}) and currents at the magnetopause (r_{DCF}) — we have used information about changes in the planetary geomagnetic cutoff rigidity system obtained by the SGS method and a simple axisymmetric model of the magnetosphere: the magnetic field is formed by the dipole geomagnetic field and two spheres with currents of opposite directions flowing along the spheres' parallels, whose magnitude is proportional to the latitude cosine [Kichigin, Sdobnov, 2017].

ANALYSIS RESULTS AND THEIR DISCUSSION

The results of the study of geoeffective events in interplanetary space, Earth's magnetosphere and atmosphere by the SGS method in late August 2005 are presented below.

Figure 1 exhibits data from direct measurements of IMF and SW parameters, calculations of variations in the isotropic flux of CRs with 4 and 10 GV rigidities at the boundary of the magnetosphere, certain angles of IMF orientation, the behavior of amplitudes of the first (A_1) and second (A_2 or CR bidirectional anisotropy) spherical harmonics of pitch-angle anisotropy of CRs with 4 GV rigidity, calculated variations of the geomagnetic cutoff rigidity in Irkutsk, as well as observed *Dst* values.

During FE-1, the maximum amplitude of the CR intensity decrease for particles with 4 GV rigidity was ~23 % at 13:00 UT; and for particles with 10 GV rigidity , ~8 % at 23:00 UT (see Figure 1, *c*). It is noteworthy that, unlike FE-1, FE-2 manifested itself only in the CR intensity with a sufficiently low particle rigidity of 4 GV, although both FEs were accompanied by strong geomagnetic storms.

Figure 1, *d*, *e* demonstrates good agreement between calculated and experimental longitude and latitude IMF orientation angles.

Table 1

Standard errors in the values under study for different NM and MT measurement errors [Kovalev et al., 2022]

$^1\delta I_{NM}$, %	$^2\delta I_{MT}$, %	$^3\delta\lambda$, degree	$^4\delta\Psi$, degree	$^5\delta A_0$, %	$^6\delta A_1$, %	$^7\delta A_2$, %	$^8\delta R_c$, GV	$^9\delta T_{SL}$, °C	$^{10}\delta T_{MA}$, °C
±0.1	±0.1	±16.9	±21.5	±1.0	±8.8	±1.7	±0.03	±1.3	±0.3
	±0.2	±16.9	±21.5	±1.0	±8.8	±1.7	±0.03	±2.5	±1.2
±0.15	±0.1	±17.0	±21.8	±1.3	±8.8	±1.7	±0.04	±1.3	±0.3
	±0.2	±17.0	±21.8	±1.3	±8.8	±1.7	±0.04	±2.5	±1.0
±0.2	±0.1	±17.5	±22.1	±1.6	±8.9	±1.8	±0.05	±1.3	±0.3
	±0.2	±17.5	±22.1	±1.6	±8.9	±1.8	±0.05	±2.5	±1.0

1, 2 — statistical errors in observational data; 3, 4 — statistical errors in determining the longitude and latitude IMF orientation angles; 5 — error in determining the CR spectrum isotropic component amplitude; 6, 7 — errors in determining the amplitude of the first and second harmonics of pitch-angle anisotropy; 8 — error in changing the planetary geomagnetic cutoff rigidity system; 9, 10 — temperature determination errors: SL — surface layer, MA — mass average.

In the model of CR modulation by heliospheric electromagnetic fields [Dvornikov et al., 2013], an increase in A_1 is observed when the IMF intensity increases. It follows from Figure 1, *f* that at certain points in time for particles with 4 GV rigidity there is strong CR anisotropy with an increase in the IMF modulus B (see Figure 1, *a*). Maximum A_1 were observed on August 24, 2005 between 09:00 and 12:00 UT (54–56 %), $|B|\approx$40 nT; on August 30, 2005, at 14:00–15:00 UT (9–16 %), $|B\approx$9 nT; and on August 31, 2005, at 04:00–08:00 UT (4–9 %), $|B|\approx$19 nT. Note that on August 24–25, 2005, A_2 (4 GV particle rigidity) grew to 4–5 % at 1–2 % background values (Figure 1, *g*). During the August 30–31, 2005 geomagnetic disturbance, A_2 increased to almost 3 % at 19:00 UT.

Since changes in the geomagnetic cutoff rigidity (ΔR_c) and the *Dst* index reflect the state of the main magnetospheric current systems, these values correlate well with each other (see Figure 1, *h*). The calculated linear correlation coefficient for August 20–31, 2005 was 0.8; for the August 24, 2005 magnetic storm and FE-1, 0.9; and for the August 31, 2005 magnetic storm and FE-2, 0.8. At the same time, maximum ΔR_c in Irkutsk during geomagnetic disturbances coincides with the maximum decrease in the *Dst* index. So, on August 24, 2005 at 12:00 UT, ΔR_c was –0.9 GV, *Dst*=–216 nT; on August 31, 2005 at 18:00 UT, –0.66 GV and –128 nT respectively.

During FEs in SW, magnetic-trap-type structures with a characteristic size of the order of 1 AU or larger (along spiral IMF) are formed in the vicinity of Earth's orbit. Similar structures can occur during propagation of high-speed SW streams. The degree of regularity of the field inside the traps is relatively high. Accordingly, the pitch-angle diffusion coefficient is low. Modulation occurs due to changes in the energy of particles as they move in regular SW fields [Dvornikov, Matyukhin, 1976].

At long transport free paths, when perturbations of motion trajectories are insignificant, the particles "feel" the energy change effect average over the trap, which in this case is negative. Here, the deceleration time for transient and trapped particles is significantly different such that the CR modulation amplitudes at large and small pitch angles also differ [Dvornikov, Matyukhin, 1979].

At certain instants of time (see Figure 1, *g*), there is high-amplitude bidirectional anisotropy of CRs in the angular distribution of high-energy particles (several GeV), which indicates, firstly, the presence of structures such as magnetic traps (with sizes from 0.1 AU to several AU), and, secondly, the smallness of the diffusion coefficient in momentum space. The bidirectional anisotropy characterized by a shortage of particles with large pitch angles is observed after particles pass through regions with increased IMF strength, as well as IMF structures either perpendicular to the Parker spiral or opposite to the background magnetic polarity. This circumstance indicates carrying-out of magnetic field loop-like structures, which, when moving away from the Sun, displace the background magnetic field, deforming it, especially at the front of medium disturbance. Penetration of CRs into and out of a magnetic trap occurs due to centrifugal and gradient drifts of particles, and the intensity decreases due to changes in the energy of CRs when they move in regular electromagnetic fields of the heliosphere.

Judging by the behavior of the IMF strength modulus and the SW velocity (see Figure 1, *a*, *b*), on August 24, Earth entered a CME region, thereby producing an FE and a magnetic storm. This is evidenced by the higher amplitude of the first harmonic of CR pitch-angle anisotropy. The increased bidirectional anisotropy on August 24–26 suggests that Earth crossed this formation with the IMF loop-like structure [Richardson et al., 2000].

On August 31, the IMF modulus increased to 15–16 nT in interplanetary space, yet no significant increases in A_1 and A_2 were detected. This fact can be explained by two reasons. Firstly, the effects of energy loss of high-energy particles and hence a decrease in their intensity occur only when the particles, before reaching Earth, cross (due to magnetic drift) a region with increased magnetic field strength. Thus, if, for example, Earth enters the southern boundary of the magnetic structure with increased field strength, and the drift velocity is directed from south to north, then the effect in high-energy CRs is not observed. Secondly, the effect of reducing the CR intensity does not occur either if the IMF loop-like structure, which is a magnetic trap, does not form. In this case, the effect of increasing the amplitude of the second harmonic is absent [Cane et al., 2001], as observed during this period.

Figure 2 displays rigidity spectra of GCR intensity variations during the geomagnetic disturbances on August 24 and 31, 2005. It can be seen that, contrary to the established opinion [Kuzmin, 1964; Krymsky, 1969], the spectra of CR variations in a wide range of rigidity from a few to tens of GV are not described by a simple power-law function $\Delta J/J \sim R^{-\gamma}$. They can thus be described only at particle rigidity over 10–15 GV. Note that in [Kuzmin, 1964; Krymsky, 1969] the conclusion that spectra of CR variations are described by a power-law function was made on the basis of studies of CR variations from muon observations at different levels in

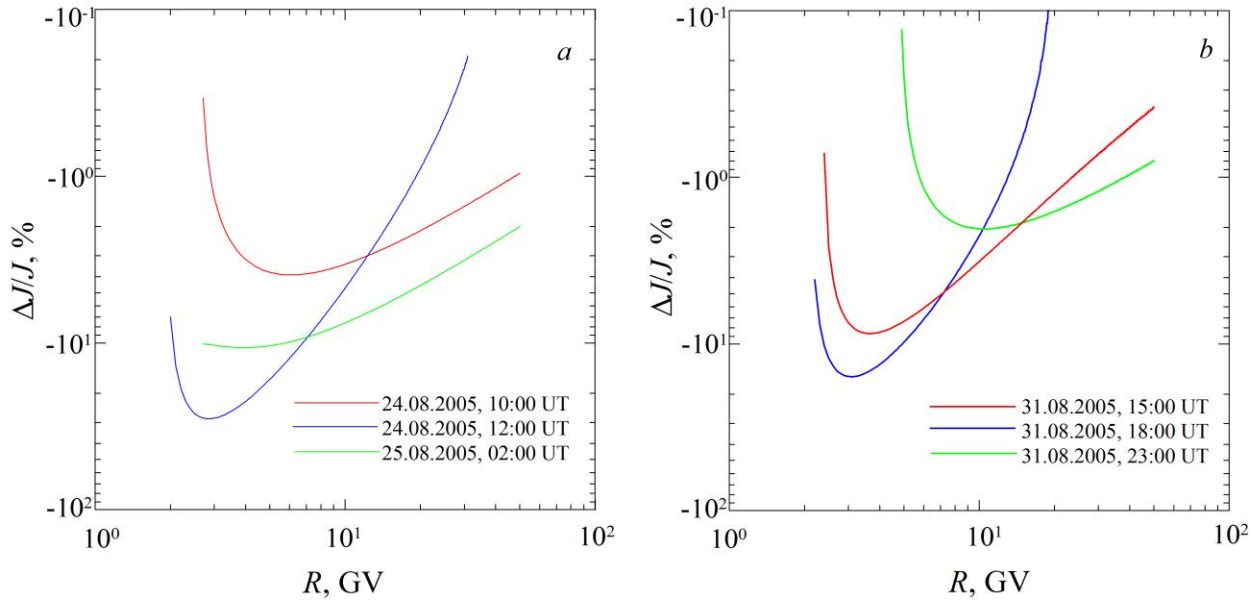

Figure 2. Rigidity spectra of CR variations for individual instants of time on August 24, 2005 (*a*) and August 31, 2005 (*b*). Spectra during different FE phases are marked with color: decrease — red line; maximum modulation — blue line; recovery — green line

the atmosphere and underground, which provide information about spectra of CR variations at particle rigidity over 10 GV.

Figure 2 shows that as an FE develops the minimum modulation spectrum shifts first to the region of lower rigidities, and then, during the recovery phase, to the region of higher rigidities. The analysis suggests that during the phase of maximum FE modulation at rigidities over 10 GV, the index of CR variation spectrum when approximated by a power-law function becomes higher than during the CR intensity decrease and recovery phases. Our calculations have shown that in the FE decrease and recovery phases the index of CR variation spectrum γ was –0.8 and –0.9 respectively. In the phase of maximum modulation, the spectrum becomes significantly softer: γ=–3.0 (for FE-1) and –5.0 (for FE-2).

Figure 3 illustrates relative variations in the CR intensity for particles with 4 GV rigidity in the geocentric solar ecliptic (GSE) coordinate system in different FE phases. Table 2 provides a description of Figure 3.

Figure 3 and Table 2 demonstrate that in the FE-1 decrease and recovery phases A_1 dominates, and in the phase of maximum CR modulation A_2 appears. The opposite situation is observed for FE-2 — A_2 dominates during the decrease and recovery phases; and A_1, during the phase of maximum CR modulation.

Dvornikov and Matyukhin [1979] examined the effect of an IMF corotating magnetic trap, which is a special case of large-scale electromagnetic fields of the heliosphere [Dvornikov et al., 2013], on the distribution

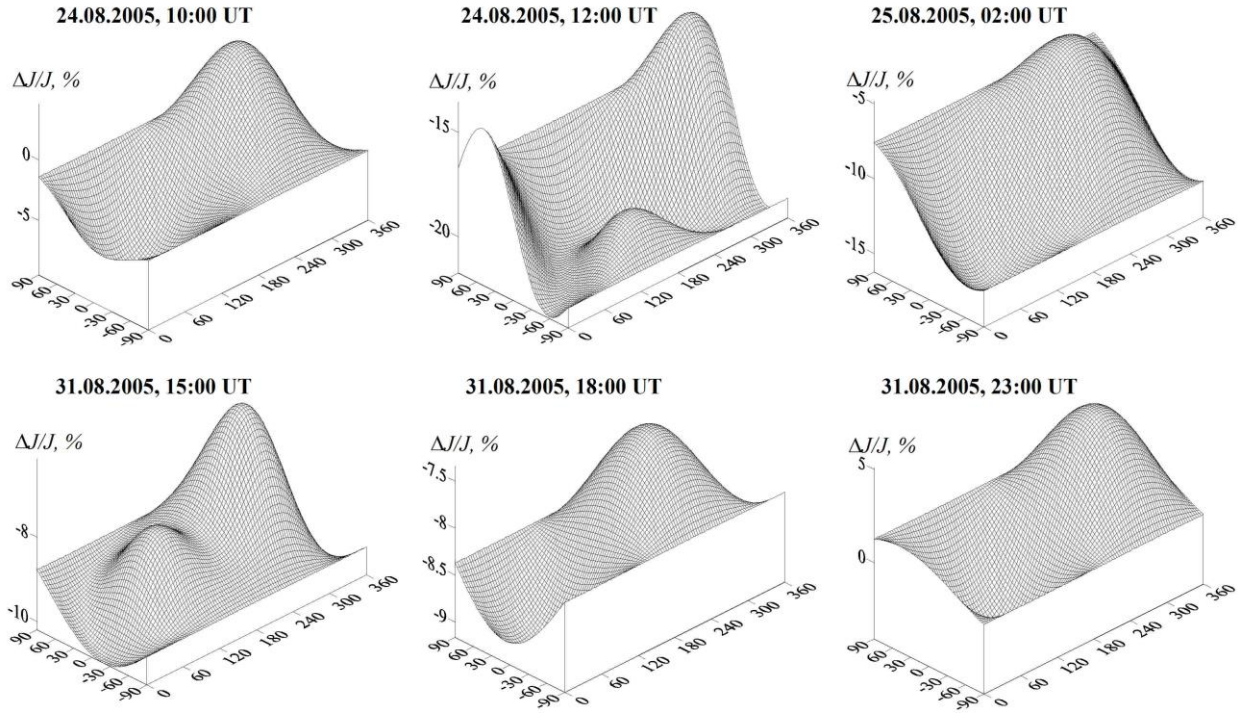

Figure 3. Relative CR intensity variations for particles with 4 GV rigidity in GSE coordinates during different FE phases (decrease phase, maximum modulation phase, and recovery phase): top panels show FE-1; bottom panels, FE-2. The X-axis is the longitude angle ψ; the Y-axis, the latitude angle λ

Table 2

Relative CR intensity variations for particles with 4 GV rigidity in the GSE coordinate system during different FE phases

FE	FE phase	Date	Time, UT	Harmonic of pitch-angle anisotropy	Flow direction (ψ — longitude, λ — latitude)
FE-1	decrease	August 24, 2005	10:00	A_1	ψ≈270°, λ≈30°
	maximum modulation	August 24, 2005	12:00	A_2	ψ≈150°, λ≈-45° and ψ≈340°, λ≈60°
	recovery	August 25, 2005	02:00	A_1	ψ≈285°, λ≈25°
FE-2	decrease	August 31, 2005	15:00	A_2	ψ≈105°, λ≈0° and ψ≈260°, λ≈15°
	maximum modulation	August 31, 2005	18:00	A_1	ψ≈240°, λ≈25°
	recovery	August 31, 2005	23:00	A_2	ψ≈105°, λ≈-75° and ψ≈285°, λ≈15°

of particles along pitch angles and showed that if transport free paths exceed the size of the trap, trapped particles significantly slow down and, accordingly, there is an anisotropic decrease in the CR intensity. Thus, Dvornikov and Matyukhin [1979] attributed the increase in A_1 and/or A_2 to IMF intensity variations and/or to the entry of Earth into the IMF loop-like structures. Consequently, the presence of bidirectional anisotropy of A_2 in the August 24 and 31, 2005 events means that Earth entered the IMF loop-like structure that is a magnetic trap.

Figure 4 presents the results of calculations of geomagnetic cutoff rigidity variations (ΔR_c) depending on its magnitude (R_c) during different phases of the August 24 and 31, 2005 geomagnetic disturbances. It follows that during the August 24 magnetic storm the ring current radius r_{DR} first decreased from 4.7 to 4.3 Earth radii (R_E) and then increased to 5.4 R_E. At the same time, the distance to the subsolar point, associated with r_{DCF}, decreased from 8.6 R_E to 6.0 R_E on August 24 at 12:00 UT, and then increased again to 9.0 R_E. During the August 31 geomagnetic storm, r_{DR} decreased from 4.8 R_E at the beginning of the event to 2.3 R_E at 23:00 UT, whereas r_{DCF} remained unchanged during this period.

Note that during maximum geomagnetic disturbances there are significant discrepancies between dependences of variation in geomagnetic cutoff rigidities on those calculated from the data obtained by the worldwide network of CR stations and by the axisymmetric model of the bounded magnetosphere with the ring current [Kichigin, Sdobnov, 2017]. At this time, other current systems are likely to appear or intensify in Earth's magnetosphere, which are not taken into account in the model we employ [Kichigin, Sdobnov, 2017].

An important feature of this work is the use of muon telescope data without temperature corrections. This makes it possible, firstly, to improve the reliability of the information obtained in the high-energy range of GCR variation spectrum and, secondly, to determine air temperature characteristics over sites of muon detectors.

Since muons form at altitudes below 13–15 km, we can gain information on the temperature at standard isobaric levels in the atmosphere from ground-based measurements of charged particles. To do this, it is necessary at each site to have observational data from CR stations equipped with muon detectors characterized by high statistical accuracy, different coupling coefficients, and density of temperature coefficients [Dorman, 1957]. In this case, the number of directions of particle arrival at a detector should significantly exceed the number of isobaric levels. Unfortunately, we do not have such devices with these characteristics, so we can only calculate the mass average temperature with adequate accuracy. In the absence of regular and fairly frequent balloon observations of atmospheric characteristics, this is important for solving a number of applied problems in various fields of science.

Figure 5 exhibits the calculated mass average air temperature over muon telescopes in Novosibirsk and Yakutsk together with direct aerological observations [ftp://arlftp.arlhq.noaa.gov/pub/archives/gdas1].

Errors in determining the mass average air temperature do not exceed ±1.2° (see Table 1). Figure 5 shows completely satisfactory agreement between the calculated mass average temperature and observational data.

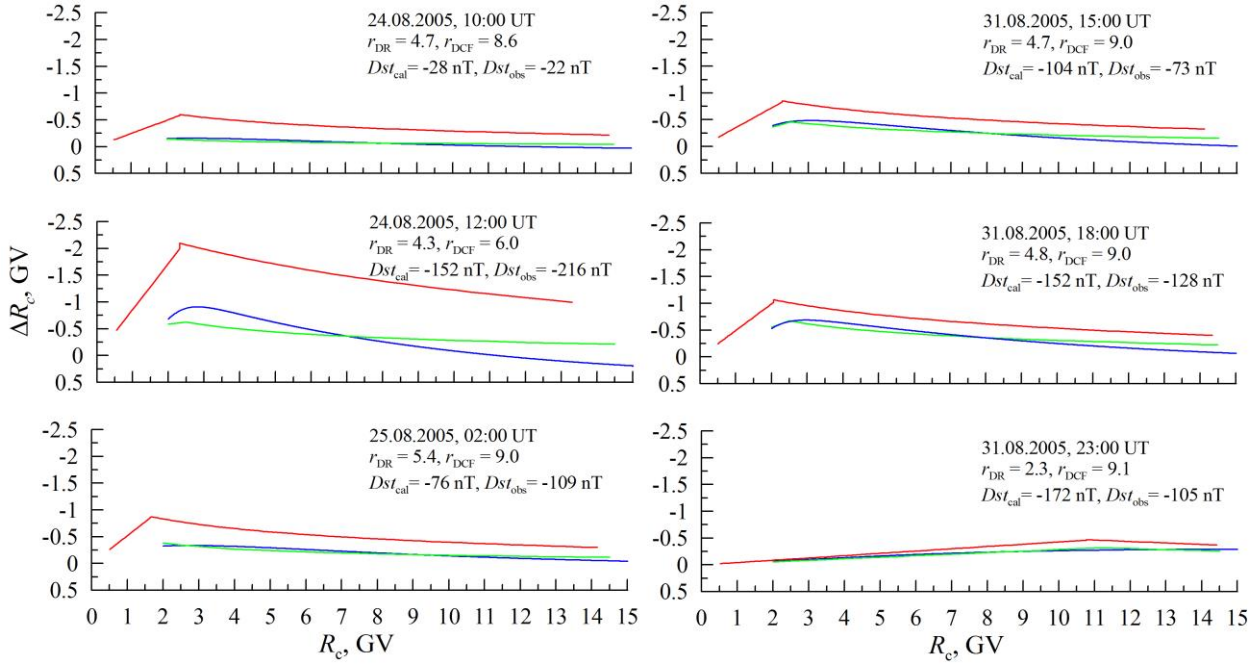

Figure 4. Variation in the geomagnetic cutoff rigidity as function of that in the initial (*a*), maximum (*b*), and recovery (*c*) phases during magnetic storms in late August 2005 (August 24, 2005 (left); August 31, 2005 (right)): the blue line indicates the results obtained by the SGS method from ground-based observations of CRs; the green line, the results of calculations by the axisymmetric model of the bounded magnetosphere; the red line, the contribution to variation in the ring current geomagnetic cutoff rigidity calculated by the axisymmetric model of the magnetosphere. On the right are date, r_{DR}, and r_{DCF}, observed and calculated *Dst* index

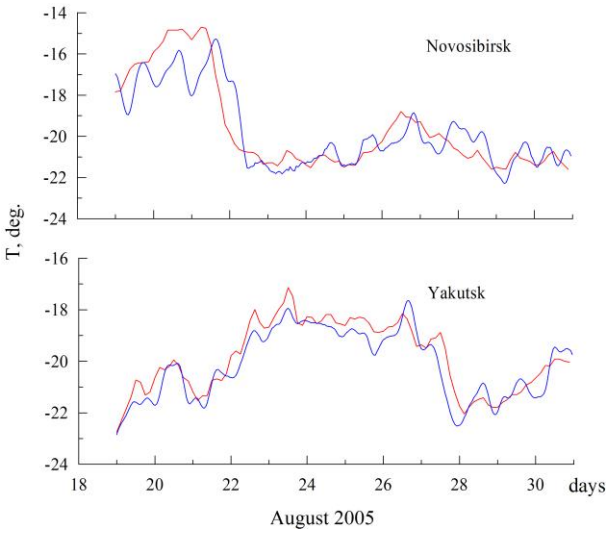

Figure 5. Time variation of the mass average air temperature in late August 2005: as calculated by the SGS method using observations over the CR stations in Novosibirsk and Yakutsk equipped with MT (blue line); observational data from [ftp://arlftp.arlhq.noaa.gov/pub/archives/gdas1] (red line)

CONCLUSION

By using ground-based observations of CRs at the worldwide network of neutron monitors with data from muon telescopes located in Yakutsk and Novosibirsk, we monitored conditions of near-Earth space, Earth's magnetosphere and atmosphere during large-scale disturbances of the interplanetary medium in late August 2005. We have identified variations of CRs with different rigidity in Earth's orbit and the amplitude of their pitch-angle anisotropy and have obtained information on IMF orientation and configuration, changes in the geomagnetic cutoff rigidity planetary system during strong geomagnetic disturbances.

We have established that during Forbush effects Earth was in SW large-scale electromagnetic fields with IMF loop-like structures.

We have determined differential rigidity spectra of CR variations in different FE phases. We have shown that these spectra are not described by a simple power law in a wide range of rigidities. This power law can describe spectra of CR intensity variations only for particle rigidities over 10 GV. At these rigidities for the FE-1 and FE-2 decrease and recovery phases, the spectral indices were $\gamma\approx-0.8$ and $\gamma\approx-0.9$ respectively, which is consistent with the conclusions drawn in [Kuzmin, 1964; Krymsky, 1969]. During maximum CR modulation, the spectra of variations at >10 GV rigidities are much softer: $\gamma\approx-3.0$ and $\gamma\approx-5.0$ respectively for the August 24 and August 31, 2005 geoeffective space weather events, despite the fact that these events differ both in the profile of CR intensity variations, observed at the stations, and in the magnitude of the magnetospheric response to SW disturbances.

During the August 24, 2005 geomagnetic disturbances, the ring current radius r_{DR} varied in the magnetic storm initial phase from 4.7 R_E to 4.3 R_E. In the recovery phase, $r_{DR}\sim5.0$ R_E. During this period, the position of the subsolar point r_{DCF} varied from ~9.0 R_E to ~6.0 R_E and returned to initial values. During the August 31 event, r_{DR} varied from ~4.7 R_E in the magnetic storm initial phase to ~2.3 R_E, whereas the position of the subsolar point ($r_{DCF}\sim9.0$ R_E) remained unchanged.

The use of MT data in the SGS method without temperature corrections, on the one hand, improves the stability of solving a system of equations in a high-energy region and, on the other hand, makes it possible to obtain the mass average air temperature over CR stations.

The work was financially supported by the Ministry of Science and Higher Education of the Russian Federation, SHICRA SB RAS (Scientific Topic FWRS-2021-0012, State Registration Number in INIS RDE 122011700180-7). The results were obtained using the equipment of Shared Equipment Center "Angara" [http://ckp-rf.ru/ckp/3056] and the Unique Research Facility "Russian National Ground-Based Network of Cosmic Ray Stations" (CRS Network) [https://ckp-rf.ru/usu/433536].

REFERENCES

Abunin A.A., Abunina M.A., Belov A.V., Eroshenko E.A., Oleneva V.A., Yanke V.G. Forbush effects with a sudden and gradual onset. *Geomagnetism and Aeronomy*. 2012, vol. 52, iss. 3, pp. 292–299.

Alania M.V., Wawrzynczak A., Sdobnov V.E., Kravtsova M.V. Temporal changes in the rigidity spectrum of Forbush. *Solar Phys.* 2013. Vol. 286. P. 561–576. DOI 10.1007/s11207-013-0273-0.

Asai A., Shibata K., Ishii T.T., Oka M., Kataoka R., Fujiki K., Gopalswamy N. Evolution of the anemone AR NOAA 10798 and the related geo-effective flares and CMEs. *J. Geophys. Res.* 2009, vol. 114, no A00A21. DOI: 10.1029/2008JA013291.

Belov A.V., Eroshenko E.A., Oleneva V.A., Struminsky A.V., Yanke V.G. What are Forbush effects caused by and what are they associated with? *Bulletin of the Academy of Sciences of USSR. Ser. Physics.* 2001, vol. 65, iss. 3, pp. 411–414.

Cane H.V., Richardson I.G., Wibberenz G., Dvornikov V.M., Sdobnov V.E. Cosmic ray evidence for magnetic field line disconnection inside interplanetary coronal mass ejections. *Proc. 27th Int. Cosmic Ray Conf.* Hamburg, Germany, August 2001. 2001, vol. 9, pp. 3531–3534.

Dvornikov V.M., Matyukhin Yu.G. Energeticheskiye poteri kosmicheskikh luchey pri dvizhenii v regulyarnom magnitnom pole solnechnogo vetra [Energetic loss of cosmic rays when moving in a regular magnetic field of the solar wind] *Izvestiya Akademii Nauk SSSR. Seriya Fizicheskaya* [Bulletin of the Academy of Sciences of USSR. Ser. Physics]. 1976, vol. 39, iss. 3, pp. 624–626. (In Russian).

Dvornikov V.M., Matyukhin Yu.G. Effekty modulyatsii kosmicheskikh luchey v korotiruyushchikh magnitnykh lovushkakh solnechnogo vetra. Izv. AN SSSR. Ser. fiz. 1979, vol. 43, iss. 12, pp. 2573–2576. (In Russian).

Dvornikov V.M., Sdobnov V.E. Time variations of the cosmic ray distribution function during a solar event of September 29, 1989. *J. Geophys. Res.* 1997, vol. 102, A11, pp. 24209–24219.

Dvornikov V.M., Kravtsova M.V., Sdobnov V.E. Diagnostics of the Electromagnetic Characteristics of the Interplanetary Medium Based on Cosmic Ray Effects. *Geomagnetism and Aeronomy.* 2013, vol. 53, no 4, pp. 430–440. DOI: 10.1134/S0016793213040075.

Dorman L.I. *Variatsii kosmicheskikh luchey* [Variations of cosmic rays]. Moscow, Gos. Izdatel'stvo tekhniko-teoreticheskoy Literatury, 1957, 492 p. (In Russian).

Forbush S.E. On the effects in the cosmic-ray intensity observed during the recent magnetic storm. *Phys. Rev.* 1937, vol. 51, pp. 1108–110.

Grigoryev V.G., Starodubtsev S.A., Dvornikov V.M., Sdobnov V.E. Estimation of the solar proton spectrum in the GLE70 event. *Adv. Space Res*. 2009, vol. 43, pp. 515–517. DOI: 10.1016/j.asr.2008.08.010.

Kichigin G.N., Sdobnov V.E. Geomagnetic cutoff rigidities of cosmic rays in a model of the bounded magnetosphere with the ring current. *Geomagnetism and Aeronomy*. 2017, vol. 57, iss. 2, pp. 132–136. DOI: 10.1134/S0016793217020049.

Kichigin G.N., Kravtsova M.V., Sdobnov V.E. Parameters of current systems in the magnetosphere as derived from observations of cosmic rays during the 2015 June magnetic storm. *Solar-Terr. Phys.* 2017, vol. 3, iss. 3, pp. 13–17. DOI: 10.12737/stp-33201702.

Kovalev I.I., Olemskoy S.V, Sdobnov V.E. A proposal to extend the spectrographic global survey method. *J. Atmos. Solar-Terr. Phys.* 2022, vol. 235, 105887. DOI: 10.1016/j.jastp.2022.105887.

Krymskiy G.F. Diffusion mechanism of diurnal cosmic-ray variations. *Geomagnetism and Aeronomy*. 1964, vol. 4, no 6, pp. 763–769.

Krymskii G.F., *Modulyatsiya kosmicheskikh luchei v mezhplanetnom prostranstve* [Cosmic ray modulation in the interplanetary space]. Moscow, Nauka Publ., 1969, 152 p. (In Russian).

Kuzmin A.I. *Variatsii kosmicheskikh luchey vysokikh energiy* [High energy cosmic ray variations]. Moscow, Nauka Publ., 1964, 126 p. (In Russian).

Liu Y., Hayashi K. The 2003 October–November fast halo coronal mass ejections and the large-scale magnetic field structures. *Astrophys. J.* 2006, vol. 640, 1135. DOI: 10.1086/500290.

Parker E.N. Cosmic ray modulation by the solar wind. *Phys. Rev*. 1958. Vol. 110, no. 6. P. 328–334.

Ptitsyna N.G., Danilova O.A., Tyasto M.I., Sdobnov V.E. Cosmic ray cutoff rigidity governing by solar wind and magnetosphere parameters during the 2017 Sep 6–9 solar-terrestrial event. *J. Atmos. Solar-Terr. Phys*. 2023, vol. 246, 106067. DOI: 10.1016/j.jastp.2023.106067.

Richardson I.G., Dvornikov V.M., Sdobnov V.E., Cane H.V. Bidirectional particle flows at cosmic ray and lower (~1 MeV) energies and their association with interplanetary coronal mass ejections/ejecta. *JGR*. 2000, vol. 105, no A6, pp. 12579–12591. DOI: 10.1029/1999JA000331.

Verma V.K. On the origin of solar coronal mass ejections. *J. Ind. Geophys. Union*. 1998, vol. 2, pp. 65–74.

URL: https://cdaw.gsfc.nasa.gov/CME_list/UNIVERSAL_ver1/2005_08/univ2005_08.html (accessed January 10, 2024).

URL: https://cdaw.gsfc.nasa.gov/CME_list/radio/waves_type2.html (accessed January 10, 2024).

URL: https://omniweb.gsfc.nasa.gov (accessed January 10, 2024).

URL: https://lweb.cfa.harvard.edu/shocks (accessed January 10, 2024).

URL: https://www.nmdb.eu (accessed January 10, 2024).

URL: https://ysn.ru/ipm/yktMT00 (accessed January 10, 2024).

URL: https://cosm-rays.ipgg.sbras.ru (accessed January 10, 2024).

URL: https://www.solarmonitor.org (accessed January 10, 2024).

URL: https://lweb.cfa.harvard.edu (accessed January 10, 2024).

URL: https://cdaw.gsfc.nasa.gov (accessed January 10, 2024).

URL: ftp://arlftp.arlhq.noaa.gov/pub/archives/gdas1 (accessed January 10, 2024).

URL: http://ckp-rf.ru/ckp/3056/ (accessed January 10, 2024).

URL: https://ckp-rf.ru/catalog/usu/433536/ (accessed January 10, 2024).

Original Russian version: Kovalev I.I., Kravtsova M.V., Olemskoy S.V., Sdobnov V.E., Starodubtsev S.A., published in Solnechno-zemnaya fizika. 2024. Vol. 10. Iss. 2. P. 29–37. DOI: 10.12737/szf-102202403.

How to cite this article

Kovalev I.I., Kravtsova M.V., Olemskoy S.V., Sdobnov V.E., Starodubtsev S.A. Monitoring of near-Earth space, Earth's magnetosphere and atmosphere during Forbush decreases in August 2005. *Solar-Terrestrial Physics*. 2024. Vol. 10. Iss. 2. P. 26–33. DOI: 10.12737/stp-102202403.